4. S. Lyapina *et al.*, *Science* **292**, 1382 (2001).
5. T. Kawakami *et al.*, *EMBO J.* **20**, 4003 (2001).
7. N. Mizushima *et al.*, *Nature* **395**, 395 (1998).
8. K. Furukawa, N. Mizushima, T. Noda, Y. Ohsumi, *J. Biol. Chem.* **275**, 7462 (2000).
9. M. Hochstrasser, *Cell* **107**, 5 (2001).
10. E. S. Johnson, A. A. Gupta, *Cell* **106**, 735 (2001).
11. A. Pichler, A. Gast, J. S. Seeler, A. Dejean, F. Melchior, *Cell* **108**, 109 (2002).
12. Y. Ichimura *et al.*, *Nature* **408**, 488 (2000).
13. Supplementary Web material, including details of certain methods, is available on *Science* Online at www.sciencemag.org/cgi/content/full/295/5564/2442/DC1.
14. Sequences were identified with the TBLASTN and the FASTA tools from the GCG package. The human sequence (UBL5) is from (*25*). Expressed sequence tag (EST) sequences were translated with the translate tool (GCG). The sequence alignment was created with the CLUSTAL algorithm (*26*).
15. R. F. Doolittle, *Of URFs and ORFs: A Primer on How to Analyze Derived Amino Acid Sequences* (University Science Books, Mill Valley, CA, 1987).
16. For mass spectrometric analysis of Hub1-protein conjugates, SDS-PAGE–purified immunoprecipitates were digested in situ overnight at 37°C with modified trypsin (Promega) at an approximate ratio of 10:1 (protein:enzyme) (*27*). Digest samples were injected onto a capillary liquid chromatography–mass spectrometry system. For details, see (*13*).
17. Strain SUB62 (*28*) was modified to express a FLAG epitope at the NH_2-terminus of Hub1 and a 3myc epitope at the COOH-terminus of Sph1. Plasmid pGD132, containing FLAG-tagged *HUB1* and its flanking sequences in a YIplac211 (*29*) backbone, was constructed by PCR. This plasmid was linearized at a Bgl II site within the 3′ untranslated region of *HUB1* and chromosomally integrated, duplicating the *HUB1* gene. Strains having lost untagged *HUB1* (yGD101) were selected on 5-FOA plates and verified by sequencing. The 3myc epitope was introduced as described (*30*). Immunoprecipitations were performed as described (*13*), except that the culture volume was 1 liter and cells were harvested at an optical density at 600 nm (OD_{600}) of 4.
18. R. A. Arkowitz, N. Lowe, *J. Cell Biol.* **138**, 17 (1997).
19. T. Roemer, L. Vallier, Y.-J. Sheu, M. Snyder, *J. Cell Sci.* **111**, 479 (1998).
20. K. Madde, M. Snyder, *Annu. Rev. Microbiol.* **52**, 687 (1998).
21. For cell polarity and mating experiments, the wild-type strain was W303 [*MAT***a** (or *MAT*α) *ura3-1 leu2-3,-112 trp1-1 his3-11 ade2-1 can1-100*]. All mutant strains were congenic and carried precise deletions of the relevant coding sequence. Cell polarity was assayed with cells grown to an OD_{600} of 0.2. α factor was added to a final concentration of 5 μM, and, after a 2-hour incubation at 30°C, cells were spread onto a microscope slide and counted. For microscopy of the GFP fusion strains, cells were grown at 25°C to an OD_{600} of 0.1 to 0.2 in rich media [yeast extract, peptone, and dextrose (YPD)]. Cells were harvested by centrifugation, washed five times with sterile water, resuspended in 40% glycerol, and placed on a microscope slide. Budding patterns were assayed by Calcofluor staining of bud scars, as described (*31*). The microscope and camera assembly have been described (*32*).
22. Cells of opposite mating type were transformed with either the YCplac111 (*MAT***a**) or YCplac33 (*MAT*α) plasmids (*29*). Cells of each mating type (3×10^6) were incubated on small (Falcon 351007) YPD plates at 30°C for the time indicated. The cells were then resuspended in sterile water, and dilution series were prepared. Mating efficiency was calculated as the ratio of colonies on selective media to those on YPD.
23. Strain construction was according to (*30*). For Sph1 tagging by GFP and 3myc, the tag was added after codon Phe^{530}. Sph1 is polymorphic (*19*), and these experiments used the short form of the protein.
24. The *S. pombe HUB1*-related gene (Fig. 1A) was amplified from a cDNA library by PCR and cloned into pGD81 (*13*) under the control of the *CUP1* promoter, using restriction sites placed on the primers. The human Hub1-related gene was similarly amplified from EST au83f03.y1. The nonconserved COOH-terminal codon (Fig. 1A) was not deleted from these coding sequences.
25. J. S. Friedman, B. F. Koop, V. Raymond, M. A. Walter, *Genomics* **71**, 252 (2001).
26. J. D. Thompson *et al.*, *Nucleic Acids Res.* **22**, 4673 (1994).
27. A. Shevchenko *et al.*, *Anal. Chem.* **68**, 850 (1996).
28. D. Finley, E. Ozkaynak, A. Varshavsky, *Cell* **48**, 1035 (1987).
29. R. D. Gietz, A. Sugino, *Gene* **74**, 527 (1988).
30. M. Knop *et al.*, *Yeast* **15**, 963 (1999).
31. J. R. Pringle, *Methods Enzymol.* **194**, 732 (1991).
32. J. Lippincott, R. Li, *J. Cell Biol.* **143**, 1947 (1998).

33. We thank R. Li, C. Kaiser, and E. Elion for advice; J. Lippincott and other members of the Li lab for assistance with various experiments; and E. Elion, D. Moazed, and members of the Finley lab for critical reading of the manuscript. Supported by NIH grants GM58223 and GM62663 (to D.F.), fellowship DI724/1-1 from the Deutsche Forschungsgemeinschaft (to G.A.G.D.), a fellowship from the Medical Foundation Charles King Trust (G.A.G.D.), and an international prize traveling fellowship 058209/Z/99/Z from the Wellcome Trust (to C.R.M.W.).

18 January 2002; accepted 22 February 2002

Senescence Induced by Altered Telomere State, Not Telomere Loss

Jan Karlseder, Agata Smogorzewska, Titia de Lange*

Primary human cells in culture invariably stop dividing and enter a state of growth arrest called replicative senescence. This transition is induced by programmed telomere shortening, but the underlying mechanisms are unclear. Here, we report that overexpression of TRF2, a telomeric DNA binding protein, increased the rate of telomere shortening in primary cells without accelerating senescence. TRF2 reduced the senescence setpoint, defined as telomere length at senescence, from 7 to 4 kilobases. TRF2 protected critically short telomeres from fusion and repressed chromosome-end fusions in presenescent cultures, which explains the ability of TRF2 to delay senescence. Thus, replicative senescence is induced by a change in the protected status of shortened telomeres rather than by a complete loss of telomeric DNA.

Replicative senescence of human cells occurs as a consequence of the progressive shortening of the TTAGGG repeat tracts at chromosome ends (*1*). Human telomeres are programmed to lose ~100 base pairs (bp) per population doubling (PD), resulting in senes-

Table 1. Effect of TRF2 on telomere shortening rates and senescence setpoints.

Cell line	PD at infection	Vector*	TRF2	Setpoint
	Telomere shortening†			
IMR90	20	112	165	
IMR90	30	104	170	
IMR90	35	100	181	
IMR90	40	99	170	
IMR90–p53-175H‡	25	95	152	
IMR90–SV40 large T	30	104	162	
IMR90–HPV16-E6 + -E7	25	97	150	
BJ	80	105	197	
	Senescence setpoint§			
IMR90	20	7.1	4.4	2.7
IMR90	30	6.1	4.1	2.0
IMR90	35	6.0	3.8	2.2
IMR90	40	6.2	4.2	2.0
IMR90 p53-175H	25	5.5	3.1	2.4
BJ	80	4.7	3.5	1.2
AG02496 A-T	~20	5.6	4.9	0.7
AG04405 A-T	~20	7.0	4.8	2.2
AG03058 A-T	~20	7.3	5.8	1.5
AG03057 A-T het.	~20	7.4	5.3	2.1

*pLPC. †Base pair per end per PD. ‡Mean length of telomeric restriction fragments (in kb) in senescent cell cultures determined by genomic blotting analysis of DNA harvested 10 days after culture growth arrest. §IMR90 cells were infected with p53-175H retrovirus at PD20 and superinfected with pLPC or TRF2 viruses at PD25; the same strategy was applied for SV40 large T (at PD25) + TRF2 (at PD30) and for HPV16-E6 + -E7 (at PD20) + TRF2 (at PD25).

cence after ~50 PDs (*2–4*). This shortening rate is faster than expected from the end-replication problem (*5–8*), suggesting active nucleolytic attack on chromosome ends. Evidence for 5′ processing lies in the presence of ~150-nucleotide 3′ overhangs at telomere ends (*9*). An overhang may be required to form a potentially protective structure at telomeres, the t loop, in which the G strand invades the duplex part of the telomere (*10*, *11*). Replicative senescence can be induced by either the p53 or the p16–retino blastoma (RB) pathways (*4*, *12*, *13*), but how these pathways are activated in cells with shortened telomeres is not known. One possibility is that senescence occurs when one or more chromosome ends have lost all telomeric DNA. The data presented here argue against this view and suggest that the main event heralding the end of the replicative life of primary human cells is a failure in the protective function of critically shortened telomeres.

TRF2 is a sequence-specific DNA binding protein that binds to the duplex array of TTAGGG repeats at human telomeres and protects chromosome ends from end-to-end fusion (*14–17*). Loss of TRF2 function leads to chromosomal abnormalities, cell cycle arrest, and the activation of the ataxia telangiectasia mutated (ATM)–p53 DNA damage response pathway (*16–18*). The protective activity of TRF2 may be related to its ability to form t loops (*10*, *11*). Retroviral-mediated overexpression of TRF2 in primary human IMR90 fibroblasts (*19*) resulted in accelerated telomere shortening (Fig. 1, A and B). Although IMR90 cells normally lose telomeric DNA at a rate of 99 to 112 bp per end per PD, TRF2 accelerated telomere attrition by 50 to 80%, from 165 to 181 bp per end per PD (Fig. 1B) (Table 1). Because there was no change in the growth rate or S-phase index (Fig. 1C), it is unlikely that the increased loss of telomeric DNA per PD was due to increased cell death or senescence. The enhanced telomere shortening explains previously recorded effects of TRF2 on telomere length maintenance in telomerase-positive cells (*20*). In contrast to the results of overexpression of TRF2, overexpression of several forms of TRF1, a related telomeric DNA binding protein, did not affect telomere shortening, even though each of these proteins was expressed at high levels and showed the expected subnuclear localization (Fig. 1, A and B) (*19*). These findings confirm the idea that TRF1 controls telomere dynamics primarily by affecting telomerase-mediated telomere elongation (*20*, *21*). Thus, TRF1 and TRF2 both act as negative regulators of telomere length but affect different aspects of telomere dynamics.

Consistent with the idea that telomere shortening is linked to DNA replication (*22*), TRF2-dependent telomere shortening required cell divisions. When the cells were temporarily arrested by contact inhibition, their telomere lengths did not change for 20

Laboratory for Cell Biology and Genetics, The Rockefeller University, 1230 York Avenue, New York, NY 10021, USA.

*To whom correspondence should be addressed. E-mail: delange@mail.rockefeller.edu

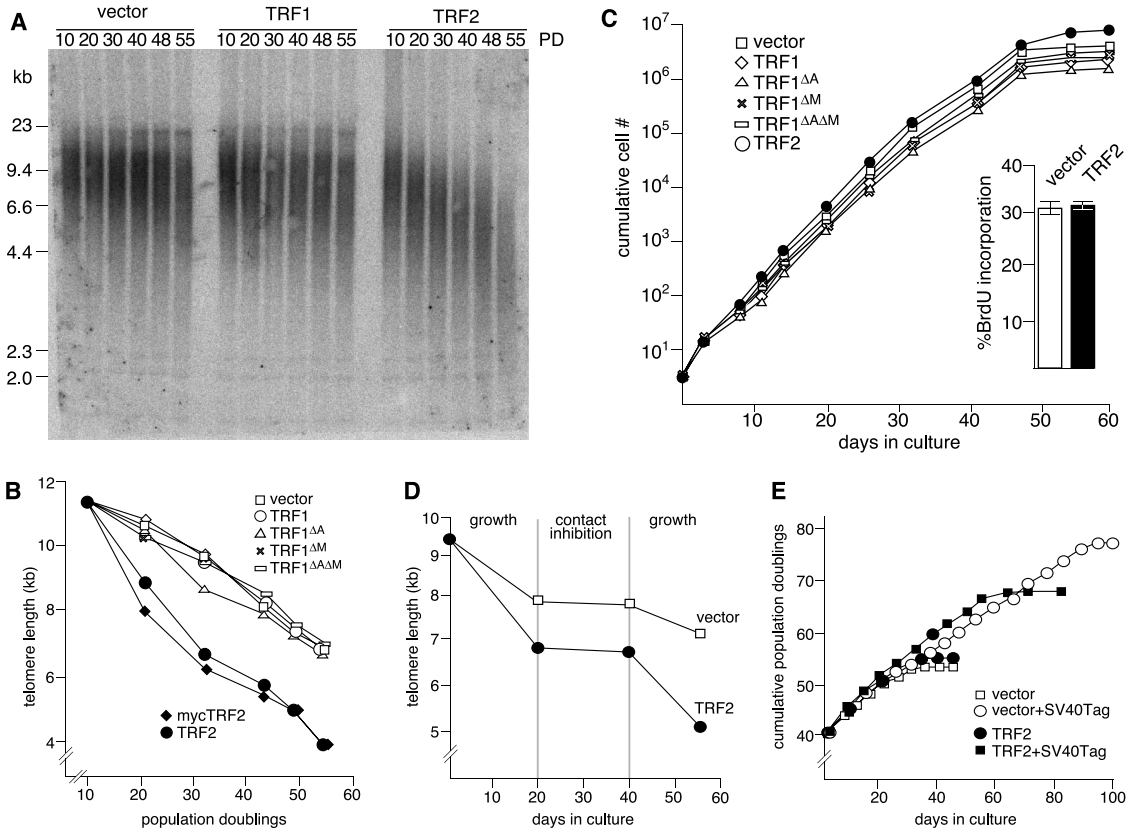

Fig. 1. Effect of TRF2 overexpression on telomere shortening and culture growth. (**A**) Genomic blotting analysis of telomeric restriction fragments in IMR90 cells expressing TRF1, TRF2, or no exogenous protein. IMR90 cells were infected at PD20 with retroviruses expressing TRF1, TRF2, or no protein (vector) (*19*). Pools of puromycin-resistant cells were passaged every 4 days by seeding 1×10^6 cells into a 15-cm dish. DNA was harvested at the indicated PDs, digested with Mbo I and Alu I, and analyzed by genomic blotting using a TTAGGG repeat probe (*19*). The lanes labeled PD10 represents cells before infection. (**B**) Graph of telomere shortening in IMR90 cells expressing the indicated TRF1 and TRF2 alleles (*19*). TRF1$^{\Delta A}$, TRF1 lacking the acidic domain; TRF1$^{\Delta M}$, TRF1 lacking the myb domain; TRF1$^{\Delta A \Delta M}$, TRF1 lacking the acidic and the myb domains. Telomeric restriction fragments were detected as in (A), and mean telomere lengths were deduced using the method described in (*19*). (**C**) Growth curve of IMR90 cells expressing the indicated genes. The cells were treated as described in (B). Cumulative cell numbers were recorded and plotted. The insert shows the percentage of cells that incorporated bromodeoxyuridine in a 1-hour interval in cultures expressing TRF2 or in vector control cells (average values and SDs are from three experiments). (**D**) Dependence of telomere shortening on proliferation. IMR90 pools infected at PD15 with the TRF2 retrovirus or with the vector control were grown for 20 days (from PDs 15 to 30) and then allowed to reach confluence. Confluent cultures were maintained for 20 days with daily media changes, reseeded at 8×10^6 cells per 15-cm dish, and grown for another 15 days (from PDs 30 to 36). Telomere lengths were measured as in (B). (**E**) Accelerated entry into crisis in TRF2-overexpressing SV40 large T–transformed cells. IMR90 cells were infected with a retrovirus expressing SV40 large T antigen and subsequently with either the TRF2 retrovirus or the vector control. After selection for both viruses, the culture growth was monitored as in (C) and plotted as cumulative PDs versus days in culture. Cells were infected with an SV40 large T retrovirus at PD35 and subsequently superinfected with a TRF2 virus. The graph starts at PD40.

days (Fig. 1D). Yet, when the culture was prompted to resume growth by reseeding, telomere shortening occurred again at the rate observed before the arrest, both in the control cells and in the cells overexpressing TRF2.

TRF2 accelerated telomere shortening in several fibroblast strains, regardless of the status of p53 or the p16-RB pathways. Inhibition of p53 with the p53-175H dominant negative allele (*23*) or suppression of both the p53 and RB pathways with viral oncoproteins (SV40 large T or HPV16-E6 and -E7) did not change the rate of telomere shortening, nor did these oncoproteins alter the ability of TRF2 to accelerate this process (Table 1). TRF2 also accelerated the entry into crisis in the SV40 large T and HPV16-E6 and -E7 cultures by ~10 PDs (Fig. 1E) (*19*). Such premature crisis is consistent with accelerated telomere shortening resulting in an earlier induction of the excessive genome damage responsible for crisis.

Accelerated telomere shortening could be explained if TRF2 enhanced the 5′ exonucleolytic processing of telomere ends, for instance by recruiting an exonuclease. Indeed, TRF2 inhibition results in a reduction in the G-strand overhang DNA, and the recruitment of a nuclease would be consistent with the protective activity of TRF2, because overhangs are required for t-loop formation (*10*, *11*, *16*). If accelerated telomere shortening were due to increased 5′ processing, the telomeres might be expected to contain longer 3′ overhangs (Fig. 2A). However, quantification of the G-strand overhang signal in TRF2-overexpressing cells showed only a minor (~15%) increase as compared to vector control cells (Fig. 2B) (*19*). If the accelerated rate of telomere shortening were entirely due to increased degradation of the 5′-ended strand, a three- to fourfold higher G-strand signal would be expected (Fig. 2A). Therefore, the effect of excess TRF2 was not only limited to the processing of the 5′-ended C strand but also involved the loss of sequences of the G-rich strand.

No premature senescence was noted in IMR90 cells that overexpressed TRF2, despite their accelerated telomere shortening. TRF2-overexpressing cells entered senescence at the same PD or later than did cells infected with TRF1 retroviruses or the vector control cultures (Fig. 1C). However, due to the rapid shortening of their telomeres, TRF2-overexpressing cells senesced with telomeres that were 2.0 to 2.7 kb shorter than those of senescent control cells (Fig. 1B) (Table 1). TRF2-expressing cells continued to grow for a considerable number of doublings (~15 PDs) beyond the normal senescence setpoint of 6 to 7 kb. The resetting of the senescence setpoint occurred regardless

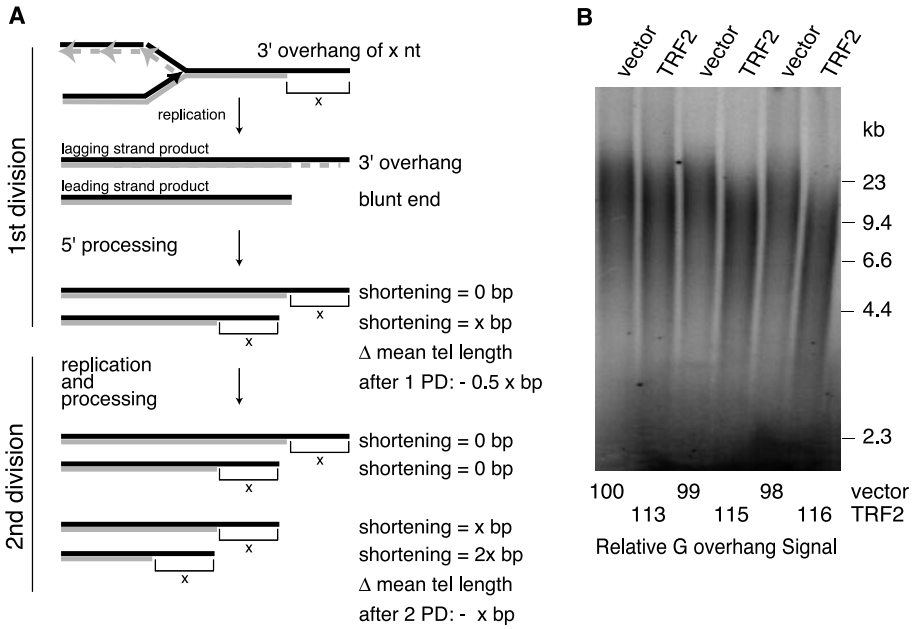

Fig. 2. TRF2 overexpression does not result in extensive elongation of the G-strand overhang. (**A**) Schematic showing the relation between the length of the telomeric overhang and the rate of telomere shortening (*24*). tel, telomere. (**B**) Quantitative analysis of telomeric G-strand overhang signals in IMR90 cells infected with the TRF2 virus or the vector control. DNA from IMR90 cells infected with the indicated viruses was harvested at 5, 10, and 15 days (from left to right) after selection, and the relative abundance of the G-strand overhang DNA was measured by quantitative annealing of an end-labeled [$(CCCTAA)_4$] oligonucleotide to equal amounts of Mbo I–Alu I digested DNA, followed by gel fractionation (*16*, *19*). Signals were quantified with a Phosphoimager and were expressed relative to the signal in the first lane.

of the time of infection of the cells and always reduced the telomere length at senescence by ~2 kb (Fig. 3A). Reduction of the senescence setpoint by 1.2 kb and a moderate life-span extension was also observed when diploid foreskin fibroblasts (BJ) were infected with the TRF2 virus (Fig. 3A) (Table 1).

Because inhibition of p53 can delay senescence, we asked whether the effect of TRF2 on the senescence setpoint was due to the repression of p53. Although overexpression of TRF2 results in a slight reduction of p53 protein levels (*19*), TRF2 could alter the senescence setpoint in p53-deficient cells. Expression of TRF2 in p53-175H cells reduced their senescence setpoint from 5.5 to 3.0 kb (Fig. 3B) (Table 1). Moreover, TRF2 lowered the senescence setpoint in A-T cells lacking ATM kinase, an upstream activator of p53 (Table 1). In addition, it is unlikely that the resetting of the senescence setpoint by TRF2 involves an effect on the RB-p16 pathway, because cells overexpressing TRF2 show normal levels and modification status of pRb and p16 (*19*).

We next considered the possibility that TRF2 acted by protecting critically short telomeres, thereby delaying the induction of senescence. Human fibroblasts lacking p53 and RB function, due for instance to the expression of HPV16-E6 and -E7, grow beyond the normal senescence setpoint (*12*, *13*). Such cells continue to lose telomeric DNA, resulting in frequent chromosome-end fusions and other chromosomal damage (*3*) (Fig. 3C). Overexpression of TRF2 in such cells created a measurable reduction in chromosome-end fusions and associated chromosomal damage (Fig. 3D), indicating that TRF2 had a protective effect on critically short telomeres. The low yield in mitotic cells from senescent cultures prohibited the direct assessment of the protective effect of TRF2 based on inspection of metaphase chromosomes from senescent cells. However, molecular data on IMR90 cells expressing p53-175H were consistent with the protection of critically short telomeres by TRF2. IMR90-p53-175H cells that are approaching replicative senescence contained a class of larger TTAGGG repeat–containing restriction fragments that resembled previously characterized telomere fusion products (Fig. 3E) (*16*). Consistent with their being derived from telomere fusions, these fragments were about twice the size of the original telomeric restriction fragments, and they lacked a G-strand overhang (Fig. 3E). When TRF2 was overexpressed, the occurrence of fused telomeric fragments was suppressed (Fig. 3E). Similarly, telomere fusion fragments were detected in normal IMR90 cells as they progressed toward senescence, whereas TRF2-overexpressing cells did not show these fragments even in the later stages of

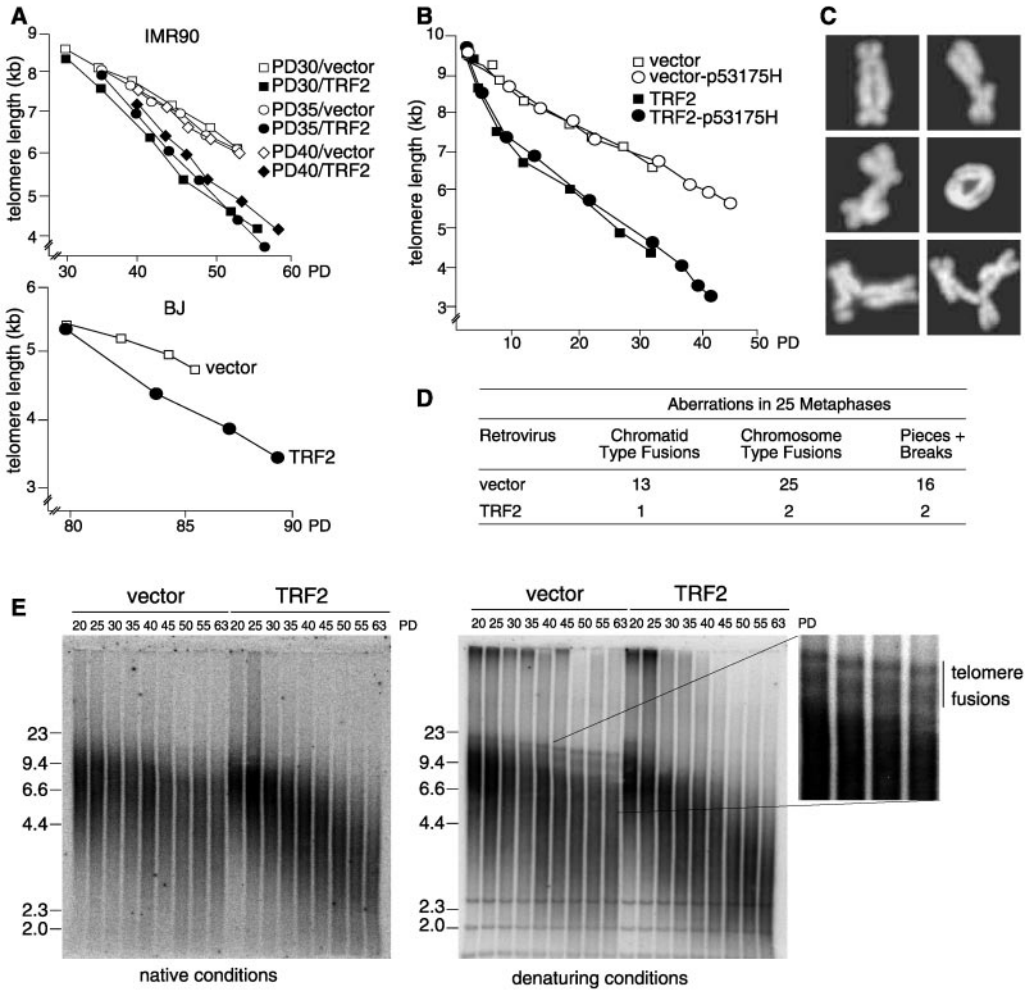

Fig. 3. Effect of TRF2 overexpression on the senescence setpoint. (**A**) Effect of TRF2 on the senescence setpoint in IMR90 and BJ cells. IMR90 and BJ cells were infected with the TRF2-expressing retrovirus or the vector control at PDs 30, 35, 40 (IMR90), and 80 (BJ); mean telomere lengths were determined as in Fig. 1 and were plotted versus PD. For each curve, the last point represents senescent cells. (**B**) Effects of TRF2 on telomere shortening and the senescence setpoint in cells with diminished p53 function. IMR90 cells were infected with a retrovirus expressing p53-175H at PD20 and were superinfected with the TRF2-expressing virus or the vector control. Mean telomere lengths were determined as in Fig. 1 and were plotted versus PD. (**C**) Examples of chromosomal aberrations observed in IMR90 cells expressing HPV16-E6 and -E7 at 10 PD before crisis. Metaphase chromosomes obtained from colcemid-treated cultures were stained with 4′,6′-diamidino-2-phenylindole (*16*). (**D**) Effect of TRF2 on chromosome-end fusions in cells with critically short telomeres. The cells described in (C) were infected with the TRF2 virus or the vector control, and the frequency of chromosome-end fusions and associated breaks and chromosome pieces was determined on metaphase spreads. (**E**) Diminished occurrence of telomere fusion fragments in p53-deficient IMR90 cells expressing TRF2. IMR90-p53-175H cells were infected as described in (B), and the telomeric restriction fragments were gel fractionated and hybridized to a ^{32}P end-labeled [(CCCTAA)$_4$] oligonucleotide under native conditions (left panel) (*19*). Subsequently, the DNA was denatured in the gel and rehybridized with the same probe (right panel).

their life-span (Fig. 1A). These data suggest that excess TRF2 can protect very short telomeres and that this is the mechanism by which TRF2 can extend the lifespan and alter the senescence setpoint of primary human cells.

Collectively, these data argue that replicative senescence in human cells is caused by a change in the status of the telomeric complex rather than by a complete loss of telomeric sequences. If the senescence signal were due to one or more chromosome ends lacking telomeric DNA altogether, TRF2 would not be expected to repress this signal and alter the senescence setpoint. One possibility is that critically shortened telomeres in senescent human cells no longer bind sufficient TRF2 to achieve a protective state, such as the t loop, a conformation that can be induced by TRF2 in vitro (*10*, *11*). Alternatively, binding of TRF2 may facilitate the recruitment of other proteins required for telomere protection and suppression of senescence. Telomere-directed replicative senescence in human cells can be induced by either the p53 pathway or the p16-RB pathway (*12*, *13*). Our data reveal that the main event activating these pathways is not the complete loss of telomeric DNA from one or more chromosome ends. Instead, telomere attrition ends proliferation by generating telomeres that are too short to function.

References and Notes

1. A. G. Bodnar *et al.*, *Science* **279**, 349 (1998).
2. C. B. Harley, A. B. Futcher, C. W. Greider, *Nature* **345**, 458 (1990).
3. C. M. Counter *et al.*, *EMBO J.* **11**, 1921 (1992).
4. J. W. Shay, W. E. Wright, *Nature Rev. Mol. Cell Biol.* **1**, 72 (2000).
5. J. D. Watson, *Nature* **239**, 197 (1972).
6. A. M. Olovnikov, *J. Theor. Biol.* **41**, 181 (1973).
7. V. Lundblad, J. W. Szostak, *Cell* **57**, 633 (1989).
8. M. S. Singer, D. E. Gottschling, *Science* **266**, 404 (1994).
9. V. Makarov, Y. Hirose, J. P. Langmore, *Cell* **88**, 657 (1997).
10. J. D. Griffith *et al.*, *Cell* **97**, 503 (1999).
11. R. M. Stansel, T. de Lange, J. D. Griffith, *EMBO J.* **20**, 5532 (2001).
12. J. W. Shay, O. M. Pereira-Smith, W. E. Wright, *Exp. Cell. Res.* **196**, 33 (1991).
13. E. Hara, H. Tsurui, A. Shinozaki, S. Nakada, K. Oda, *Biochem. Biophys. Res. Commun.* **179**, 528 (1991).
14. D. Broccoli, A. Smogorzewska, L. Chong, T. de Lange, *Nature Genet.* **17**, 231 (1997).
15. T. Bilaud *et al.*, *Nature Genet.* **17**, 236 (1997).
16. B. van Steensel, A. Smogorzewska, T. de Lange, *Cell* **92**, 401 (1998).
17. J. Karlseder, D. Broccoli, Y. Dai, S. Hardy, T. de Lange, *Science* **283**, 1321 (1999).
18. T. de Lange, *Oncogene* **21**, 532 (2001).
19. Supplementary material is available on *Science* Online at www.sciencemag.org/cgi/content/full/295/5564/2446/DC1.
20. A. Smogorzewska *et al.*, *Mol. Cell. Biol.* **20**, 1659 (2000).
21. B. van Steensel, T. de Lange, *Nature* **385**, 740 (1997).
22. R. C. Allsopp *et al.*, *Exp. Cell. Res.* **220**, 194 (1995).
23. P. W. Hinds *et al.*, *Cell Growth Differ.* **1**, 571 (1990).
24. K. E. Huffman, S. D. Levene, V. M. Tesmer, J. W. Shay, W. E. Wright, *J. Biol. Chem.* **275**, 19719 (2000).

25. We thank S. Lowe for retroviral vectors and advice, D. Galloway for HPV16-E6 and -E7 retrovirus, G. Hannon for SV40 large T retrovirus, J. Shay for aged BJ cells, K. Kuchler for 9E10 antibodies, and members of the de Lange lab for comments on the manuscript. Supported by the Ellison Medical Foundation and NIH grants CA76027 and AG16643 (T.d.L.), the Cornell/RU/MSKCC Tri-Institutional MD/PhD program (A.S.), and the Human Frontier Science Program and Charles H. Revson Fellowships (J.K.).

3 January 2002; accepted 15 February 2002